Journal of Materials Chemistry C

Accepted Manuscript

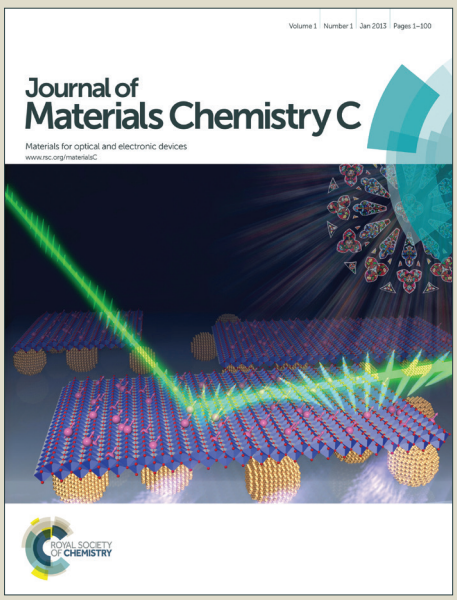

ROYAL SOCIETY OF CHEMISTRY

www.rsc.org/materialsC

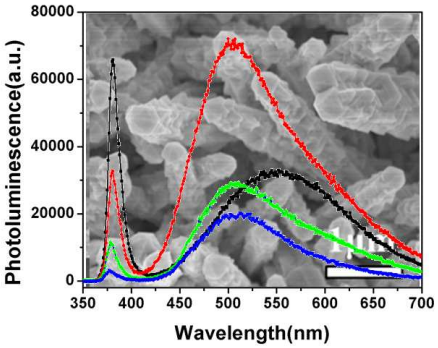

Gas-phase anion exchange was employed to convert ZnO nanorods into ZnO/ZnSe heterostructure or pure ZnSe nanorods. The product showed intensive visible light emission, which was attributed to the V_{Zn}-related defect complexes in ZnO core.

Cite this: DOI: 10.1039/c0xx00000x

www.rsc.org/xxxxxx

ARTICLE TYPE

Gas-Phase Anion Exchange towards ZnO/ZnSe Heterostructures with Intensive Visible Light Emission

Yan Wang[a], Meng-Xia Liu[a], Tao Ling[a], Cheng-Chun Tang[b],Chun-Yi Zhi [c,] and Xi-Wen Du[a,]*

Received (in XXX, XXX) Xth XXXXXXXXX 20XX, Accepted Xth XXXXXXXXX 20XX

DOI: 10.1039/b000000x

Gas-phase anion exchange favors the formation of highly crystalline and metastable nanostructures which may possess superior properties. In the present work, we employed the gas-phase anion exchange to convert ZnO nanorods into ZnSe nanostructures. We found that the thick ZnO nanorods transformed into ZnO/ZnSe core/shell structure with a zinc blende ZnSe shell via nucleation and growth of ZnSe nanoparticles, while the thin ones could directly template the growth of pure WZ-ZnSe nanorods. The ZnO/ZnSe heterostructure shows intensive green emission, which arises from the V_{Zn}-related defect complexes in ZnO core.

Introduction

One-dimensional (1D) semiconductor nanostructures (e. g. nanowires, nanorods, and nanobelts) exhibit many advantages and are regarded as well-defined building blocks for constructing nanodevices.[1,2] ZnSe is a well-known semiconductor with a direct band gap (2.67 eV) and a large exciton binding energy (21 meV).[3-6] It possesses two polymorphs, zinc-blende (ZB) and wurtzite (WZ) structures. The former is a stable structure at room temperature, and the latter is metastable but with improved optical properties.[7,8] Therefore, ZnSe nanowires with WZ structure are highly anticipated for light emitting diodes, solar cells, photodetectors. [3-6] Moreover, ZnSe can work with ZnO to construct heterojunctions for device application, taking advantages of both fast charge separation and quick carrier transfer between the two semiconductors with different energy levels.[9,10]

Many methodologies have been developed to prepare ZnO/ZnSe core/shell nanowires, e.g., chemical transformation,[11] chemical vapor deposition,[10,12] pulsed laser deposition[9] and successive ionic layer adsorption and reaction.[13] Among them, chemical transformation via ion exchange can convert one structure to another facilely, and is considered efficient for achieving desirable morphologies, compositions, and especially, non-equilibrium nanostructures.[14-31] Plenty of previous studies have been focused on converting ZnO nanowires into ZnSe nanostructures via solution-based anion exchange.[11,32-34] However, the products by wet chemical route are usually polycrystalline particles with ZB phase structure.[11,32,33,35] The reason may exist that the process is based on a dissolution-recrystallization mechanism.[32,33]

Compared with solution-based ion exchange, gas-phase anion exchange is usually conducted at high temperature (>400 ºC). In this process, thermal disturbance can provide sufficient kinetic energy for promoting anion exchange but preserving the phase structure of template material, which facilitates high crystallinity and metastable phase structures.[12,36,37] Until now, only a few reports demonstrated the anion exchange of nanowires in vapor.[37-43] For example, ZnO nanowires were converted to core-shell ZnO/ZnS and pure ZnS nanowires,[37] and $W_{18}O_{49}$ nanowires were transformed into W_2N nanowires.[44]

Based on above, we propose that gas-phase anion exchange is feasible for producing highly crystalline ZnSe nanostructures. Herein, we first prepare ZnO nanorod arrays, and then conduct anion exchange in selenium vapor, as a result, we obtain ZnO/ZB ZnSe core/shell nanorods and pure WZ ZnSe nanorods by using thick (300~500 nm) and thin (~60 nm) ZnO nanorods, respectively, as starting materials. The morphology, phase structure and the composition of ZnO/ZnSe heterostructures are characterized by scanning electron microscope (SEM), X-ray diffraction (XRD), transmission electron microscope (TEM) and energy dispersive X-ray spectroscopy (EDS), respectively. The formation mechanism is systematically investigated by observing the structural evolution during the anion exchange. In particular, the product exhibits excellent optical properties which are very promising for optoelectrical devices.

Experimental

Synthesis of ZnO nanorods

Firstly, TiO_2 seed layer was deposited on fluorine-doped tin oxide (FTO) glass by immersing the substrate in 0.05 M ethanol solution of tetrabutyl orthotitanate for 30 s at room temperature and then dried by N_2 flow, the immersion and drying were repeated for three times. Then the substrates with TiO_2 seed layer were annealed at 500 º C for 1 h. For the synthesis of thick ZnO nanorods, a precursor solution was prepared by dissolving 0.01 mol zinc nitrate hexahydrate [$Zn(NO_3)_2{\cdot}6H_2O$] and 0.01 mol hexamine, respectively, in 200 mL deionized water, and then

mixing two solutions. FTO substrate was placed in a 50 mL Teflon-liner stainless steel autoclave with 30 mL precursor solution. Hydrothermal synthesis was conducted at 100 ºC for 9 h, afterwards, the FTO glass substrates were taken out, washed with distilled water and ethanol, and then dried in air. The thin ZnO nanorods were obtained via the same procedure but dissolving 0.005 mol $Zn(NO_3)_2{\cdot}6H_2O$ in 200 mL deionized water.

Gas-phase anion exchange of ZnO nanorods

The gas-phase anion exchange of ZnO nanorods was performed in a tube furnace. FTO substrate with ZnO nanorods and 0.02 mol Se powder were placed at the centre and the end of heating area of the tube furnace, respectively, then the tube was pumped to a pressure of 500 Pa, and heated up to 600 ºC at a heating rate of 10 ºC/min, the corresponding temperature of Se powder position was measured as 467 ºC. The temperature was kept for 0, 10, and 60 min, respectively, at 600 ºC, finally the furnace was cooled down to room temperature naturally.

Characterization

The morphology of samples was observed by using a Hitachi S-4800 scanning electron microscope (SEM) with an energy dispersive spectrometer (EDS) module and a FEI TechnainG2 F20 transmission electron microscope (TEM) with a field-emission gun operating at 200 kV. The crystal structure of the products was investigated in a Bluke D8 advance X-ray diffractometer (XRD). A UV-Visible absorption (Abs) spectrophotometer (Hitachi U-3010 spectrophotometer) was used to measure the absorbance of samples. Photoluminescence (PL) spectra were acquired at room temperature with an excitation wavelength of 325 nm in Jobin Yvon FluoroLog-3 fluorescence spectrometer.

Results and discussion

The thick ZnO nanorods exhibit a hexagonal contour with diameters varying from 300 to 500 nm, as shown in SEM image (Figure 1a). XRD result shown in Figure 1h reveals that the starting material only contains ZnO, and the peaks related to SnO_2 originate from the FTO substrate.

After the ZnO nanorods were heated to 600 ºC in selenium vapor, their morphology and structure evolved with holding time. Once the temperature reached 600 ºC, many nanoparticles formed on the tip and side walls of ZnO nanorods (Figure 1b). A new weak peak appeared around 27° in XRD pattern, and it belongs to ZB ZnSe (JCPDS no.37-1463). EDX linescan analysis across a nanoparticle illuminates that the nanoparticle contain high concentrations of Se and Zn elements (Figures S1a and S1b in supporting information). Fast Fourier transfer (FFT) pattern of a high resolution TEM (HRTEM) image can be indexed to belong to a [110] ZB structure (Figure S1c in supporting information). All of the above results suggested that ZB ZnSe nanoparticles formed on the surface of ZnO nanorods immediately after the temperature reached 600 ºC.

After the temperature was held at 600 ° C for 10 min, the number and size of nanoparticles increased obviously (Figure 1c). Simultaneously, the diffraction peaks related to ZB ZnSe increased in XRD pattern (Figure 1h). As the temperature was held up to 60 min, the nanoparticles connected and grew into a hexagram-like contour (Figure 1d), which could be seen more clearly in side-view (Figure 1e) and the top-view SEM images (Figure 1f). Figure 1g showed a top-view image of a broken nanorod, which revealed that the products possessed a core-shell structure with nonuniform shell thickness varying from 80 to 200 nm. The XRD pattern of 60 min sample exhibited intensive ZB ZnSe peaks as well as ZnO peaks, indicating many ZB ZnSe formed during the temperature-holding process.The positions of the peak of zinc blende ZnSe around 27° in the top three patterns of Figure 1h are slightly different from e ach other. The slight shift of the peak position arises from the interface stress between ZnO core and ZnSe shell.[12]

.

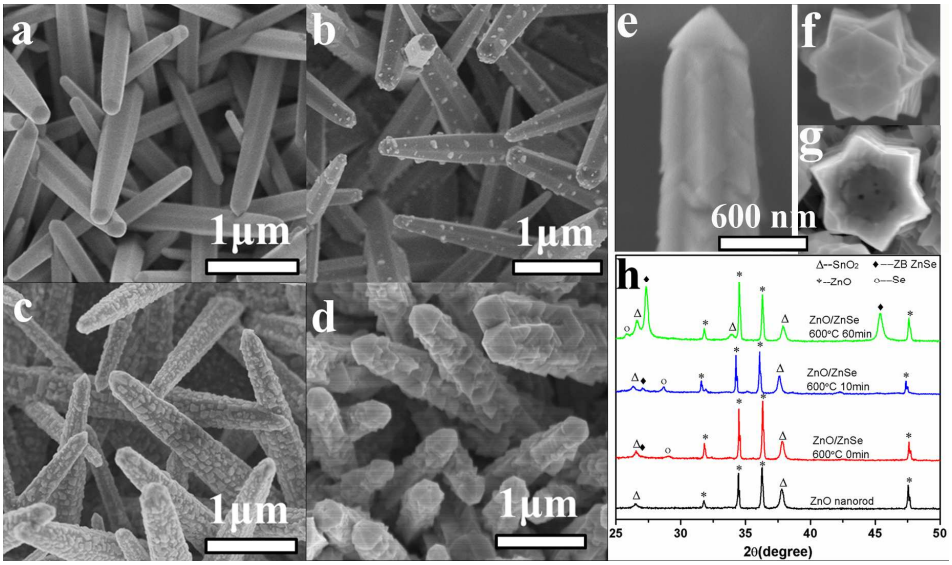

Fig. 1. Time-dependent morphological and structural evolution of ZnO nanorods in anion exchange process. SEM images of (a) initial ZnO nanorods, (b) the sample heated to 600 ºC without holding temperature, (c) the sample being kept temperature at 600 ºC for 10 min, (d) the sample being kept temperature at 600 ºC for 60 min.(e) side view of a nanorod in (d), (f) top-view of a nanorod in (d), (g) top-view of a broken nanorod. (h) XRD patterns of the samples shown in (a)~(d).

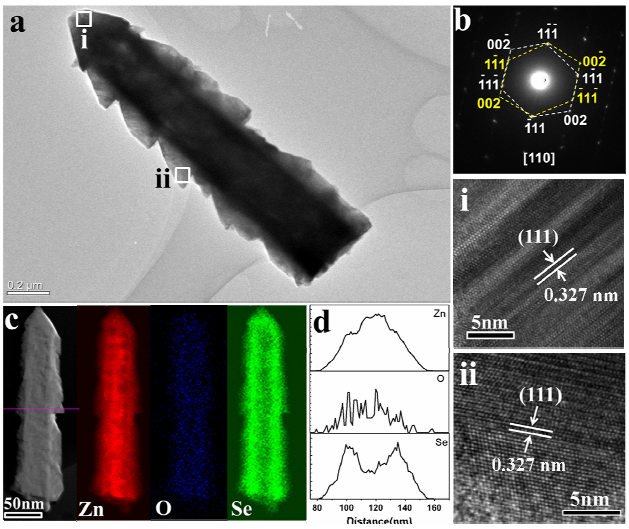

Fig. 2. Structural and compositional characterizations of the sample being kept temperature at 600 ºC for 60 min. (a) TEM image, (i) and (ii) are HRTEM images of the areas labeled in (a); (b) SAED pattern of nanorod in (a); (c) STEM and corresponding Zn, O, Se elemental mapping images of a single nanorod; (d) line scan profiles along the line shown in STEM image in (c).

The microstructure of the ZnO/ZnSe core/shell nanorods was further characterized by using TEM. Figure 2a shows a low-magnification TEM image where the product displayed sawtooth sides and a triangular head.The selected area electron diffraction (SAED) pattern taken from a nanorod exhibits two sets of single crystal diffraction pattern that are symmetric and share [$\bar{1}$ 11] and [1 $\bar{1}$ $\bar{1}$] spots at the zone axis of [110] ZB-ZnSe(Figure 2b). This pattern indicates a twinning structure with (111) twin planes.[45] Figures 2i and 2ii clearly illustrate the HRTEM image of the twins taken at the side wall and the tip of a nanorod (Figures 2i and 2ii correspond to the regions i and ii, respectively, in Figure 2a). The lattices parallel to the twin boundary show an interplanar spacing of 0.327 nm, which accords to the value of (111) planes of ZB-ZnSe, [46] suggesting that the twins are (111) type.

Elemental mapping and linescan analysis were conducted to investigate the elemental distribution in the nanorods. Figure 2c shows that the product only contains Zn, O and Se elements. In linescan profiles (Figure 2d), Zn element distribute equally across the core and the shell, while two Se peaks appear at the shell regions, confirming the formation of a ZnSe outer layer.

When thin ZnO nanorods with diameters less than 60 nm (see Figures 3a and 3b) were employed as the template, pure ZnSe nanorods with WZ structure were obtained (Figures 3c and 3d), as shown in supporting information Figure S2), the product exhibits same orientation along [0001] with WZ ZnO template (Figure 3d). On the other hand, some ZnSe nanoparticles are found in the product; however, they possess a ZB phase structure (see supporting information Figure S3). The nanoparticles are supposed to grow up by the reaction of sublimated ZnO with Se_2 vapor. Although the reaction conditions are identical, ZB phase rather than WZ phase is obtained due to the absence of WZ ZnO template. These results indicate that the formation of WZ ZnSe arises from template effect of WZ ZnO nanorods.

We also observed some cavities inside ZnO core or at the

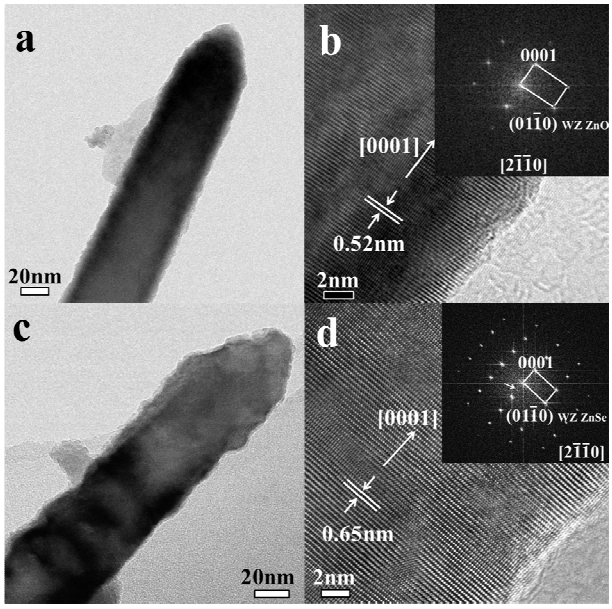

Fig. 3. (a) TEM image of the ZnO nanorod with a diameter about 60 nm; (b) HRTEM image of the ZnO nanorod shown in (a), the inset is the corresponding fast Fourier transformation (FFT) pattern; (c) TEM image of a nanorod in the product by anion exchange; (d) HRTEM image of the nanorod in (c), the inset is the corresponding FFT pattern

interface between ZnO core and ZnSe shell after anion exchange, and the cavity sizes increase with the temperature-holding time at 600 ºC (Figure 1g in main text and Figures S4a, S4b, and S4c in supporting information), which provided clues for the atomic diffusion during the anion exchange. This phenomenon is likely to occur through the outward diffusion of Zn and O atoms in the ZnSe shell, while the inward diffusion of Se atoms are blocked by the ZnSe shell, as a result, core ZnO material suffers a net loss, leading to the formation of the cavities.[43]

On the basis of the above, we propose a model for the growth of coaxial nanorods by gas-phase anion exchange, and the graphical illustration is presented in Figure 4. For the thick ZnO nanorods, Se powder in the low-temperature zone was evaporated at the initial stage, and Se_2 vapor diffused to the high-temperature zone where the anion exchange took place. Although the stability of ZnO is superior to ZnSe at room temperature,[47,48] theoretical calculation demonstrates that ZnSe becomes thermodynamically stable over ZnO at high temperature, e. g. 800 K. [42] On the other hand, the high temperature enhances the thermal vibration of ZnO lattice, which favours the outward diffusion of Zn and O atoms. Subsequently, a reaction takes place on the surface of ZnO nanorods, [42]

$$4ZnO(s) + 3Se_2(g) \rightarrow 4ZnSe(s) + 2SeO_2(g) \quad (1)$$

where Se_2 vapour discriminates into Se^{2-} and Se^{4+} ions and combined with Zn^{2+} and O^{2-} ions, respectively. As a result, ZnSe islands with a stable ZB structure nucleate and grow up. The ZnSe islands gradually connect each other to form a continuous shell, which inhibits the further diffusion of reactive Ions (Zn^{2+},

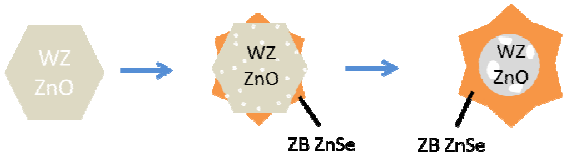

Fig. 4. Schematic illustration of the growth mechanism for ZnO/ ZB ZnSe coaxial nanorod.

O^{2-} and Se^{2-}). Finally, the ZnSe shell stops growing when the ZnSe shell thickness reaches the diffusion mean-free path of reactive ions. Resultantly, a coaxial core-shell structure is obtained. On the other hand, many vacancies are left in the ZnO core due to the loss of Zn^{2+} and O^{2-} ions, they aggregate and form visible cavities during the temperature-holding stage.

When the thin ZnO nanorods are employed as the starting material, the interdiffusion of Zn^{2+}, O^{2-} and Se^{2-} ions can proceed sufficiently because the ZnO nanorod diameter (~60 nm) is less than the diffusion mean-free path of reactive ions (~80 nm). The WZ ZnO nanorods then template the growth of ZnSe nanords via the anion exchange, and the product inherits the single-crystal WZ structure of ZnO nanorods. Such a mechanism is totally distinct from the case of thick ZnO nanorods.

To evaluate optical properties of the products, Abs and PL spectra are collected at room temperature; and the results were shown in Figure 5. In Figure 5a, thick ZnO nanorods show an intrinsic absorption edge around 390 nm, and an energy gap of 3.21 eV is determined by extrapolating linear part of the $(\alpha h\nu)^2$-$h\nu$ plot till its intersection with the $h\nu$-axis (Figure S5a). After the anion exchange reaction, a new absorption step emerges at 470 nm and increased with the anion exchange time (Figure 5a). The $(\alpha h\nu)^2$-$h\nu$ plot corresponding to the samples after anion exchange suggests a new band gap of 2.60 eV (Figures S5b, S5c). Considering that the ZB-ZnSe forms after anion exchange, we then assign the 2.61 eV to that of ZB phase. Similar results were reported by Shan et al.[49]

In the PL spectra, pure ZnO exhibits a relatively sharp UV emission (about 381 nm) ascribed to excitonic recombination at the near-band edge (NBE), together with a broad deep-level emission centered around 550 nm.[50] After being heated to 600 ºC but without temperature-holding, the coaxial nanorods exhibit a dramatically enhanced asymmetric emission around 505 nm, and the UV emission becomes weak obviously. Further anion exchange causes a gradual fall in the PL intensity of both visible and UV emissions.

We also tested the optical properties of the pure ZnSe sample obtained by selenizing thin ZnO nanorods, and the results were shown in Figure S6. The sample emits very weak light, and no obvious peak can be found in the spectrum.

Next, we discuss the PL evolution of the coaxial nanorods with reaction time. The UV (381 nm) and yellow (550 nm) PL peaks from the starting ZnO nanorods can be ascribed to excitonic recombination at the near-band edge and the excess zinc (e.g. zinc interstitial) close to or on the surface, respectively.[51] As the ZnO nanorods was slowly heated to 600 ºC, the excess zinc and even the Zn^{2+} ions in the lattice diffuse outward and react with

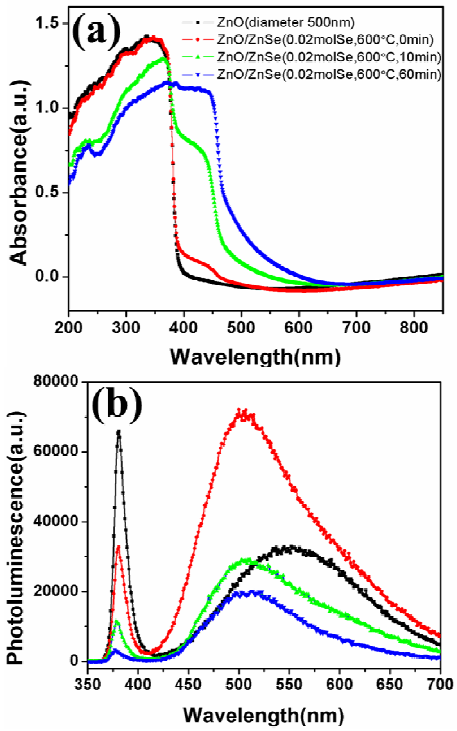

Fig. 5. Abs and PL spectra of the products with different reaction time. The PL spectra were acquired at an excitation wavelength of 325 nm.

Se^{2+} generated by the disproportionation of Se_2 vapour, while the diffusion of O^{2-} ions is more difficult due to their bigger size and the relatively low temperature during the heating stage. Therefore, a large amount of defect complexes related to Zn vacancy (V_{zn}) are generated in the ZnO nanorods, which are regarded to be responsible for the green emission of 505 nm in literatures, [52, 53] After being held at 600 ºC for a longer time, the excess oxygen can diffuse out of ZnO nanorods, leading to the formation of many cavities in ZnO core, simultaneously reducing the number of V_{Zn}-related defect complexes and then weakening the green emission. On the other hand, the produced ZnSe layer cannot give visible light emission (which can be proved by the PL properties of pure ZnSe sample composed of both WZ ZnSe nanorods and ZB ZnSe nanoparticles, see Figure S4), therefore, the total PL intensity of coaxial nanorods is remarkably depressed.

Conclusions

ZnO/ZB-ZnSe coaxial nanorods and pure WZ-ZnSe nanorods were fabricated by anion exchange of thick and thin ZnO nanorods, respectively, in selenium vapor. The microstructural evolution during the anion exchange was investigated by SEM, TEM, XRD and elemental analysis. We find that the thin WZ-ZnO nanorods can directly template the growth of WZ-ZnSe nanorods via thorough interdiffusion and direct exchange of anions (O^{2-} and Se^{2-}), while the thick ones do not favour the diffusion and reacted in a different way, namely, the Zn^{2+} cations diffuse outward and react with Se^{2-} anions at the surface of ZnO nanorods, hence ZnSe nanoparticles with ZB structure nucleate, grow up, and finally connect into a continuous shell. The

ZnO/ZnSe heterostructure shows intensive green emission, which arises from the V_{Zn}-related defect complexes due to the loss of Zn^{2+} anions at the beginning of the heating stage. We believe that the gas-phase anion exchange can be applied to different material systems for fabricating various heterostructures with promising properties for optoelectronic or photocatalysed applications.

Acknowledgements

This work was supported by The National Basic Research Program of China (2014CB931703), the Natural Science Foundation of China (Nos. 51171127, 51102176, 51271129 and 11272229), Natural Science Foundation of Tianjin City (Nos. 11ZCKFGX01300, 11JCYBJC02000 and 09JCZDJC22600) and Seed Foundation of Tianjin University

Notes and references

[a] *Tianjin Key Laboratory of Composite and Functional Materials, School of Materials Science and Engineering, Tianjin University, Tianjin 300072, P. R. China*
[b] *School of Material Science and Engineering, Hebei University of Technology, Tianjin 300130, China*
[c] *Department of Physics & Materials Science,City University of Hong Kong 83 Tat Chee Avenue Kowloon, Hong Kong SAR, China*
**Author to whom any correspondence should be addressed.*
E-mail: xwdu@tju.edu.cn

1. J. T. Hu, T. W. Odom and C. M. Lieber, *Acc. Chem. Res.*, 1999, **32**, 435-445.
2. M. S. Gudiksen, L. J. Lauhon, J. Wang, D. C. Smith and C. M. Lieber, *Nature*, 2002, **415**, 617-620.
3. B. Xiang, H. Z. Zhang, G. H. Li, F. H. Yang, F. H. Su, R. M. Wang, J. Xu, G. W. Lu, X. C. Sun, Q. Zhao and D. P. Yu, *Appl. Phys. Lett.*, 2003, **82**, 3330-3332.
4. U. Philipose, H. E. Ruda, A. Shik, C. F. de Souza and P. Sun, *J. Appl. Phys.*, 2006, **99,** 066106..
5. J. A. Zapien, Y. K. Liu, Y. Y. Shan, H. Tang, C. S. Lee and S. T. Lee, *Appl. Phys. Lett.*, 2007, **90**, 213114.
6. B. Goswami, S. Pal, C. Ghosh and P. Sarkar, *J. Phys. Chem. C*, 2009, **113**, 6439-6443.
7. S. B. Qadri, E. F. Skelton, A. D. Dinsmore, J. Z. Hu, W. J. Kim, C. Nelson and B. R. Ratna, *J. Appl. Phys.*, 2001, **89**, 115-119.
8. Z. W. Wang, L. L. Daemen, Y. S. Zhao, C. S. Zha, R. T. Downs, X. D. Wang, Z. L. Wang and R. J. Hemley, *Nature Mater.*, 2005, **4**, 922-927.
9. K. Wang, J. Chen, W. Zhou, Y. Zhang, Y. Yan, J. Pern and A. Mascarenhas, *Adv. Mater.*, 2008, **20**, 3248-3253.
10. J. J. Zheng, Z. M. Wu, W. H. Yang, S. P. Li and J. Y. Kang, *J. Mater. Res.*, 2010, **25**, 1272-1277.
11. L. L. Chen, W. X. Zhang, C. Feng, Z. H. Yang and Y. M. Yang, *Ind. Eng. Chem. Res.*, 2012, **51**, 4208-4214.
12. Z. M. Wu, Y. Zhang, J. J. Zheng, X. G. Lin, X. H. Chen, B. W. Huang, H. Q. Wang, K. Huang, S. P. Li and J. Y. Kang, *J. Mater. Chem.*, 2011, **21**, 6020-6026.
13. J. Chung, J. Myoung, J. Oh and S. Lim, *J. Phys. Chem. Solids*, 2012, **73**, 535-539.
14. G. D. Moon, S. Ko, Y. Min, J. Zeng, Y. N. Xia and U. Jeong, *Nano Today*, 2011, **6**, 186-203.
15. F. Dawood and R. E. Schaak, *J. Am. Chem. Soc.*, 2009, **131**, 424-425.
16. A. M. Smith and S. M. Nie, *J. Am. Chem. Soc.*, 2011, **133**, 24-26.
17. Y. F. Yu, J. Zhang, X. Wu, W. W. Zhao and B. Zhang, *Angew. Chem., Int. Ed.*, 2012, **51**, 897-900.
18. X. Wu, Y. F. Yu, Y. Liu, Y. Xu, C. B. Liu and B. Zhang, *Angew. Chem., Int. Ed.*, 2012, **51**, 3211-3215.
19. P. H. C. Camargo, Y. H. Lee, U. Jeong, Z. Q. Zou and Y. N. Xia, *Langmuir*, 2007, **23**, 2985-2992.
20. J. M. Pietryga, D. J. Werder, D. J. Williams, J. L. Casson, R. D. Schaller, V. I. Klimov and J. A. Hollingsworth, *J. Am. Chem. Soc.*, 2008, **130**, 4879-4885.
21. J. Park and S. W. Kim, *J. Mater. Chem.*, 2011, **21**, 3745-3750.
22. B. Mukherjee, A. Peterson and V. Subramanian, *Chem. Commun.*, 2012, **48**, 2415-2417.
23. J. M. Luther, H. M. Zheng, B. Sadtler and A. P. Alivisatos, *J. Am. Chem. Soc.*, 2009, **131**, 16851-16857.
24. H. Li, R. Brescia, R. Krahne, G. Bertoni, M. J. P. Alcocer, C. D'Andrea, F. Scotognella, F. Tassone, M. Zanella, M. De Giorgi and L. Manna, *ACS Nano*, 2012, **6**, 1637-1647.
25. K. Miszta, D. Dorfs, A. Genovese, M. R. Kim and L. Manna, *ACS Nano*, 2011, **5**, 7176-7183.
26. B. Sadtler, D. O. Demchenko, H. Zheng, S. M. Hughes, M. G. Merkle, U. Dahmen, L. W. Wang and A. P. Alivisatos, *J. Am. Chem. Soc.*, 2009, **131**, 5285-5293.
27. R. D. Robinson, B. Sadtler, D. O. Demchenko, C. K. Erdonmez, L. W. Wang and A. P. Alivisatos, *Science*, 2007, **317**, 355-358.
28. B. Zhang, Y. Jung, H. S. Chung, L. Van Vugt and R. Agarwal, *Nano Lett.*, 2010, **10**, 149-155.
29. A. Som and T. Pradeep, *Nanoscale*, 2012, **4**, 4537-4543.
30. H. McDaniel, J. M. Zuo and M. Shim, *J. Am. Chem. Soc.*, 2010, **132**, 3286-3288.
31. J. Park, H. Zheng, Y. W. Jun and A. P. Alivisatos, *J. Am. Chem. Soc.*, 2009, **131**, 13943-13945.
32. S. Cho, J. W. Jang, J. Kim, J. S. Lee, W. Choi and K. H. Lee, *Langmuir*, 2011, **27**, 10243-10250.
33. S. Cho, J. W. Jang, S. H. Lim, H. J. Kang, S. W. Rhee, J. S. Lee and K. H. Lee, *J. Mater. Chem.*, 2011, **21**, 17816-17822.
34. P. Chen, L. Gu and X. B. Cao, *CrystEngComm*, 2010, **12**, 3950-3958.
35. S. Cho, J. W. Jang, J. S. Lee and K. H. Lee, *Nanoscale*, 2012, **4**, 2066-2071.
36. X. Huang, M. Wang, M. G. Willinger, L. D. Shao, D. S. Su and X. M. Meng, *ACS Nano*, 2012, **6**, 7333-7339.
37. S. K. Panda, A. Dev and S. Chaudhuri, *J. Phys. Chem. C*, 2007, **111**, 5039-5043.
38. L. Dloczik, R. Engelhardt, K. Ernst, S. Fiechter, I. Sieber and R. Ko□nenkamp, *Appl. Phys. Lett.*, 2001, **78**, 3687.
39. L. Dloczik and R. Konenkamp, *Nano Lett.*, 2003, **3**, 651-653.
40. L. Dloczik and R. Koenenkamp, *J Solid State Electrochem.*, 2004, **8**, 142-146.
41. I. Y. Y. Bu and Y.-M. Yeh, *Ceram. Int.*, 2012, **38**, 3869-3873.
42. D. Lee and K. Yong, *Mater. Chem. Phys.*, 2012, **137**, 194-199.
43. L. Neveux, D. Chiche, D. Bazer-Bachi, L. Favergeon and M. Pijolat, *Chem. Eng. J.*, 2012, **181-182**, 508-515.
44. J. Thangala, Z. Chen, A. Chin, C.-Z. Ning and M. K. Sunkara, *Cryst. Growth Des.*, 2009, **9**, 3177-3182.

45. Y. Myung, J. H. Kang, J. W. Choi, D. M. Jang and J. Park, *J. Mater. Chem.*, 2012, **22**, 2157-2165.
46. M. Den Hertog, M. Elouneg-Jamroz, E. Bellet-Amalric, S. Bounouar C. Bougerol, R. Andre´, Y. Genuist, P. Poizat, K. Kheng, and S. Tatarenko, *J. Appl. Phys.*, 2011, **110**, 034318, 1-9.
47. I. Ohkubo, A. Ohtomo, T. Ohnishi, Y. Mastumoto, H. Koinuma and M. Kawasaki, *Surface science*, 1999, **443**, L1043-L1048.
48. S. B. Zhang, S.-H. Wei, A. Zunger and H. Katayama-Yoshida, *Phys. Rev. B*, 1998, **57**, 9642-9656.
49. C. X. Shan, Z. Liu, X. T. Zhang, C. C. Wong and S. K. Hark, *Nanotechnology*, 2006, **17**, 5561-5564.
50. H. M. Xiong, Y. Xu, O. G. Ren and Y. Y. Xia, *J. Am. Chem. Soc.*, 2008, **130**, 7522-7523.
51. E. De la Rosa, S. Sepulveda-Guzman, B. Reeja-Jayan, A. Torres, P. Salas, N. Elizondo and M. J. Yacaman, *J. Phys. Chem. C,* 2007**, 111**, 8489-8495.
52. K. H. Tam, C. K. Cheung, Y. H. Leung, A. B. Djurisic, C. C. Ling, C. D. Beling, S. Fung, W. M. Kwok, W. K. Chan, D. L. Philips, L. Ding and W. K. Ge *J. Phys. Chem. B,* 2006, **110**, 20865-20871.
53. E. S. Jung, J. Y. Lee and H. S. Kim, *J. Korean Phys. Soc.*, 47, 2005, S480-S484.